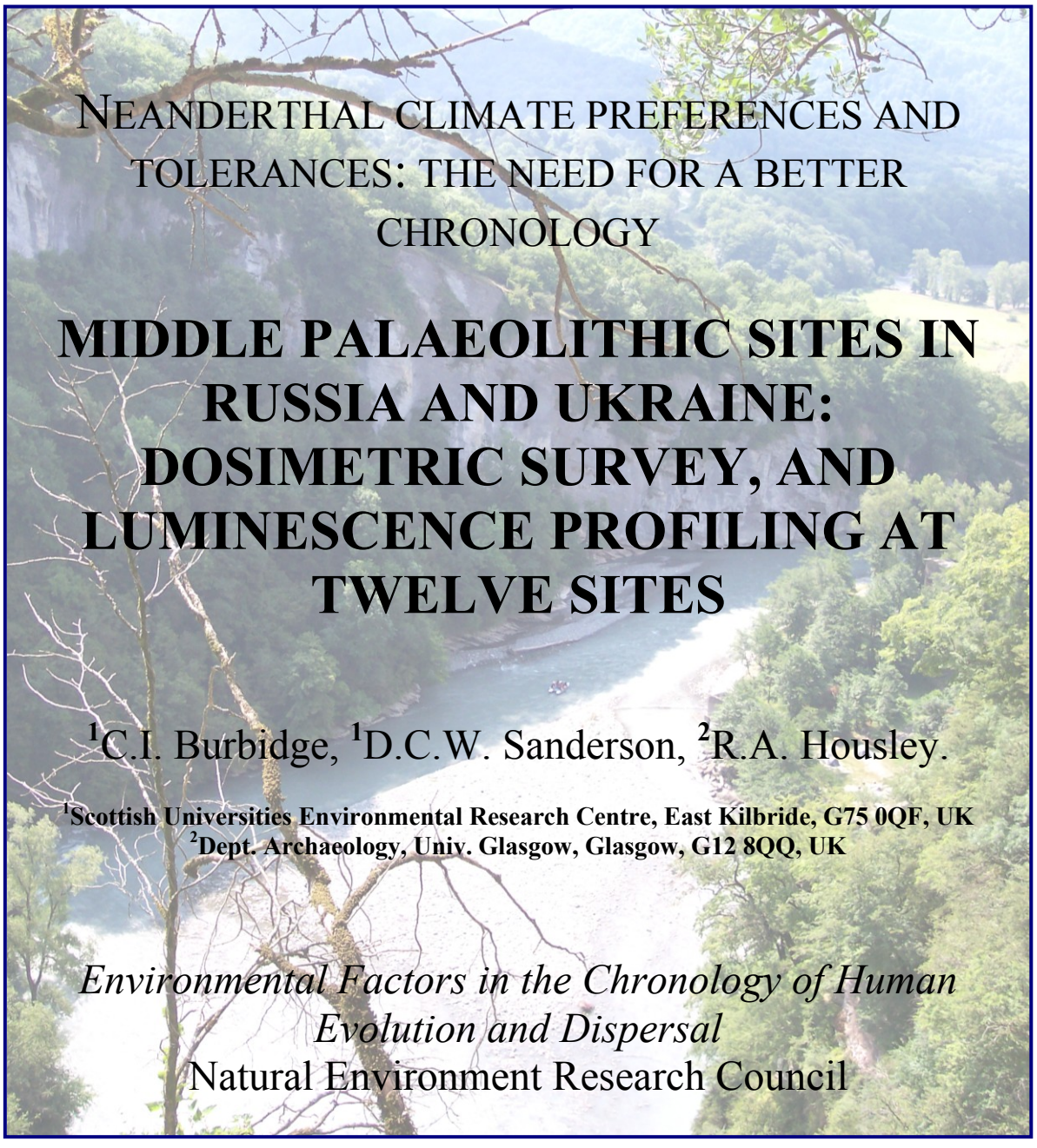

Scottish Universities Environmental Research Centre

NEANDERTHAL CLIMATE PREFERENCES AND TOLERANCES: THE NEED FOR A BETTER CHRONOLOGY

MIDDLE PALAEOLITHIC SITES IN RUSSIA AND UKRAINE: DOSIMETRIC SURVEY, AND LUMINESCENCE PROFILING AT TWELVE SITES

[1]C.I. Burbidge, [1]D.C.W. Sanderson, [2]R.A. Housley.

[1]Scottish Universities Environmental Research Centre, East Kilbride, G75 0QF, UK
[2]Dept. Archaeology, Univ. Glasgow, Glasgow, G12 8QQ, UK

Environmental Factors in the Chronology of Human Evolution and Dispersal
Natural Environment Research Council

East Kilbride Glasgow G75 OQF Telephone: 01355 223332 Fax: 01355 229898

Contents

Figures

Tables

1 Introduction

Post fieldwork prioritisation of the 15 sites sampled in the 2004 field season yielded a shortlist of six for the initial focus of luminescence investigations (Burbidge *et al*., 2005, Section 1.4). These were Kostienki 14, Kabazi II, Akhshtyr, Biriuchya Balka 2 and 1a, and Monasheskaya (Figure 1.1). The main criteria used for selection were the size of a site's diagnostic artefact assemblage, the presence of human remains, the presence of evidence for both Upper and Middle Palaeolithic site usage, the potential to provide good pollen and/or faunal proxies, time-depth and integrity of the stratigraphy, the quality of existing chronological indicators, and the potential for dating using luminescence techniques. It was recognised that the shortlist should include examples from each of the different regions sampled, and of a range of site types (open, cave, etc.), and as the more important sites in each region came to the fore, these latter criteria were satisfied as a consequence of the general selection process.

During the period of initial luminescence investigation, arrangements were made to date samples from Kabazi V by TL on burnt flint (D. Richter, Max Plank Institute for Palaeoanthropology), and AMS ^{14}C on bone (Oxford Accelerator Laboratory). AMS ^{14}C samples were also submitted from Navalishenskaya and Malaya Vorontsovskaya. These three sites were thus added to the list of sites for initial luminescence investigations. Gubs Rockshelter 1 and Barakaevskaya were then included, to examine their relationship to Monasheskaya. Also, although Karabai figured low on the initial prioritisation list, it was expected to be amenable to luminescence dating on geomorphological grounds, and samples were examined during the development of luminescence sample preparation procedures.

Of the fifteen site sampled then, eleven were the subject of initial luminescence investigations. These have been based around the measurement of "luminescence profiles". During fieldwork, relatively large numbers of small sediment samples were taken at most sites, to encompass the majority of sedimentary contexts in the sampled sections (Burbidge *et al*., 2005, sections 1.2.1, 2.2, 3.2, 4.2, 5.2). Different mineral and grain size dominated fractions have been separated from these samples in the laboratory, and subjected to basic measurements to provide indications of the sediments' behaviours with respect to luminescence dating. Comparisons of results up and down the profiles, and with independent sedimentological information, has then been used to make inferences about the datability of the sediments as a whole, about the optimal mineral/grain size fraction to use for dating, and about sedimentological processes that have operated at each site.

In parallel with the luminescence profiling of selected sites, high resolution gamma spectrometry has been conducted on sediment purposely collected in association with the "full" luminescence dating samples (Burbidge *et al*., 2005, sections 1.2.1, 2.2, 3.2, 4.2, 5.2). Measurements have been made on every sample collected, to estimate the contributions of emissions from different radionuclides to the dose absorbed by each sample during its burial. This was designed to facilitate assessment of the presence and potential importance of radioactive disequilibrium, spatial inhomogeneity (by comparison with field gamma spectrometry), and approximate dose rate values to aid interpretation of the profiling results.

Figure 1.1. The region northeast of the Black Sea, showing the location of all sites sampled in the 2004 field season.

2 High resolution gamma spectrometry survey

A survey of the radionuclides present in the sampling locations for luminescence dating has been conducted using high resolution gamma spectrometry, with the aims of estimating the potential importance of radioactive disequilibrium, spatial inhomogeneity (by comparison with field gamma spectrometry), and approximate values of dose rate.

A luminescence age is calculated by dividing the radiation dose absorbed by a sample during its burial, by the average dose rate to it during that time (Eqn. 1). The dose rate to a sample is a function of the radioactivity of its burial environment, the vast majority of which is generally produced by Potassium-40 (^{40}K) and the Uranium (^{238}U, ^{235}U) and Thorium (^{232}Th) decay series. Radioactive disequilibrium and spatial inhomogeneity of radioactivity both complicate determination of the average dose rate to a luminescence sample during its burial.

Eqn. 1 $$Age(a) = \frac{D_e(Gy)}{DoseRate(Gy/a)}$$

In a radioactive decay series in equilibrium, the rate of decay of daughter isotopes will appear the same as that of the parent, since production of the daughters is controlled by the (half life of the) parent. If the series is in disequilibrium the decay rates appear different down the series, though this is often expressed as differences in apparent parent concentration (calculated assuming equilibrium). Disequilibrium occurs when elements in the decay series are moved in or out of the sample volume, and is therefore indicative of changes in radioactivity, and hence dose rate, with time. Movement of isotopes is facilitated if they are gaseous or soluble in water, but the effects of any movement "event" are mitigated if the remainder of the series can return to equilibrium quickly (i.e. if the mobile isotope and its daughters have short half lifes). Conversely, the effects of disequilibrium in antiquity are easier to measure if long lived isotopes were affected.

The most problematic decay series, in terms of changes in dose rate during the period of interest to the present study (~20 ka - ~150ka), is that of ^{238}U. This contains soluble Uranium and Radium isotopes with relatively long half lives, and gaseous ^{222}Rn with a half life of 3.8 days: short enough to return to equilibrium quickly with respect to the period of interest, but long enough to allow significant movement if not sealed within a mineral grain or sedimentary matrix. Further, a large proportion of the dose rate from the ^{238}U series arises from the daughters of ^{222}Rn (α: 57%, β: 60%, γ: 98%). However, in the elemental proportions commonly observed in sediments (1 ppm U : 3 ppm Th : 1% K), the Uranium series only contributes a large proportion of the dose rate from alpha radiation (α: 54%, β: 14%, γ: 17%). Inaccuracies of greater than ~5% in the estimation of overall dose rate to a luminescence sample are therefore only likely to occur in cases of extreme disequilibrium, or where Uranium is present in unusually high concentrations relative to Potassium and Thorium. The latter case is in itself an indicator of potential disequilibrium arising from the movement of Uranium isotopes.

Spatial inhomogeneity of radioactivity produces inaccuracies in dose rate determinations only if the measured sample is insufficiently representative of the radiation environment of the material used for luminescence measurements during its burial. The range of gamma radiation in soil means that material with contrasting radioactivity may substantially affect the average dose rate to a sample if it is within ~20 cm, equivalent to around 50 kg of sediment. Laboratory gamma spectrometry measurements are necessarily made on much smaller samples (of the order 100 g), so comparison with *in-situ* gamma dose rate measurements can indicate the significance of radioactive inhomogeneity at a site, and hence whether (the less precise) *in-situ* measurements would be preferred to laboratory determinations.

Spatial inhomogeneity of beta and alpha dose rates also complicates dose rate determination. These have very different ranges to gamma radiation in soil, and hence relate to very different masses of sample (α: ~10 μm, ~10^{-8} g. β: ~1 mm, ~10^{-2} g). Their small ranges make the effects of spatial variations in alpha and beta radiation on luminescence dating results difficult to quantify. However, gamma measurements may be used to indicate the presence of materials with contrasting radioactivities and/or particular larger scale patterns in radioisotope concentration. Based on this, a qualitative assessment of a site/sample's propensity for problems with alpha and beta inhomogeneity may indicate particular sample locations or mineral/grain-size

fractions or approaches to measurement to use in order to minimise the effects of such inhomogeneity.

2.1 Methods

The loose sediment purposely collected from around each of the full luminescence dating samples ("Lab γ" Burbidge *et al.*, 2005, Appendices 2.2, 3.2, 4.2, 5.2) was first dried at 50 °C, and *in-situ* water content determined as the mass lost by drying as a proportion of the dry sediment mass. The dry sediment was then crushed using a rotary mill, and 100 g from each sample weighed into PP bottles identical to each other, and to that containing 100 g of milled Shap Granite reference material (Sanderson, 1986). The milled sediments were then tamped down to a similar depth as the Shap, such that the geometry of the samples was similar to that of the reference material: 60 mm diameter x 23 mm depth. Thus, only differences in self-absorption at low gamma energies might affect the comparability of samples and reference material: this depends on the average atomic weight of the material, which is expected to vary in the range 20 to 25 u (for Clay, e.g. $Al_4Si_4O_{10}(OH)_8$ and Calcite, $CaCO_3$ respectively). At low energies, between 30 and 100 keV, this range would produce differences in self-absorption of the order ±30 % relative to the Shap Granite reference material (Figure 2.1). The lids of the bottles were then sealed on using epoxy resin, and the samples were stored for at least 1 month prior to measurement, to allow the daughters of any ^{222}Rn in Radon gas escaping from the freshly milled sample to return to equilibrium.

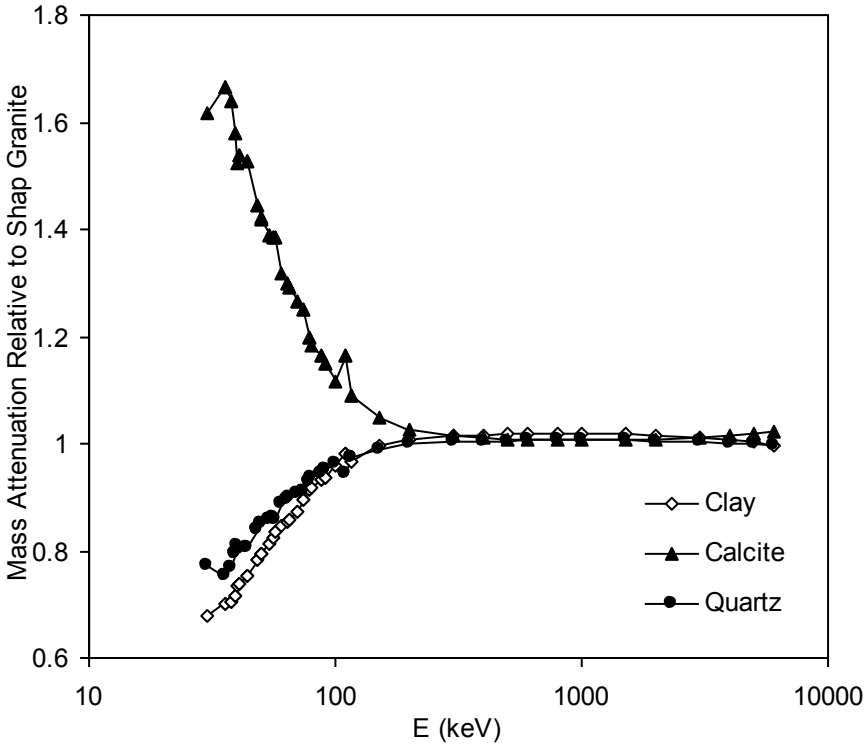

Figure 2.1. Mass attenuation coefficient vs. energy for common materials in the EFCHED samples, as a proportion of that for the Shap Granite used as a reference material for gamma spectrometry in the SUERC laboratory. Shap elemental composition from O'Brien *et al*. (1985).

Samples were measured for between 25 ks and 75 ks (7-21 hrs), between June and October 2005, on either of two high-resolution gamma spectrometers in the SUERC laboratory ("Detector 2" and "Detector 3"). Both detectors are Ortec model 918 buffer, with liquid nitrogen cooled, 50% relative efficiency, hyperpure Ge semiconductor crystals in copper-lined lead shielding. Spectra were recorded and processed using Ortec "Maestro" MCA software. The Shap reference material was measured once weekly on each spectrometer when samples were being measured, and backgrounds (with no bottle present) were measured over weekends. Region of interest (ROI) files were defined using the Shap and background measurements, to estimate the intensities of peaks in photon counts associated with the energies of gamma emissions from ^{40}K and various radioisotopes in the U and Th decay series. The radioisotopes, emission energies, and regions of interest for each detector are listed in Table 2.1. Note that the regions of interest differ at low energies from the 1 keV per channel energy calibration defined using higher energy peaks, as a result of small differences in cooling and coupling between crystal and electrodes.

Isotope	Half Life	Emission		Region Of Interest (keV)	
		Energy (keV)	Intensity	Detector 2	Detector 3
Potassium					
40-K	1.28e9 a	1460.8	0.107	1454 - 1466	1454 - 1466
Uranium Series					
238-U	4.47e9 a				
234-Th	24.1 d	62	0.0402	60 - 67	66 - 74
		92.6	0.054	89 - 97	95 - 102
226-Ra**	1599 a	185.99	0.0328	183 - 190	185 - 193
214-Pb	26.8 m	241.91	0.0745	* - *	* - *
		295.2	0.191	291 - 298	291 - 298
		351.9	0.369	348 - 356	348 - 356
214-Bi	19.9 m	609.3	0.468	604 - 614	605 - 615
		1120.28	0.154	1114 - 1124	1114 - 1126
		1238	0.061	1232 - 1243	1232 - 1244
		1764.5	0.162	1758 - 1769	1758 - 1770
		2204	0.052	2198 - 2208	2193 - 2213
210-Pb	22 a	45	0.045	43 - 51	50 - 56
Thorium Series					
232-Th	1.405e10 a				
228-Ac	6.15 h	338.7	0.12	335 - 342	334 - 343
		911.3	0.29	906 - 917	906 - 918
		964.84	0.0545	957 - 974	954 - 974
		969.16	0.1746	957 - 974	954 - 974
224-Ra	3.62 d	240.987	0.0397	* - *	* - *
212-Pb	10.64 h	238.625	0.434	232 - 246	235 - 250
212-Bi	1.01 h	727.2	0.0675	723 - 732	721 - 733
208-Tl	3.06 m	277.358	0.0637	273 - 281	274 - 284
		583.19	0.851	578 - 588	579 - 589
		860.56	0.126	856 - 864	857 - 867
		2614.5	0.999	2606 - 2619	2607 - 2620

* counted in the same ROI as 212-Pb
**includes a weak emission from 235-U

Table 2.1. Radioisotopes and their emissions measured using gamma spectrometry in the present study. The energy regions used to determine the peak intensities in each measurement are shown for both detectors.

To calculate apparent parent concentrations for each peak, and infinite matrix dose rates for each sample, background count rates in each region of interest were first

subtracted from both Shap and sample count rates. Parent concentrations in the sample were then scaled to those of Shap according to the ratio of net count rates (Eqn. 2). From these, infinite matrix dose rates were calculated using the conversion factors in Table 2.2.

Eqn. 2. $$Conc_{sample} = Conc_{shap}\left(\frac{CtRt_{sample} - CtRt_{background}}{CtRt_{shap} - CtRt_{background}}\right)$$

Conversion Factors

Specific Activity / Concentration

	K (Bq/kg/%K)	U (Bq/kg/ppmU)	Th (Bq/kg/ppmTh)
	309	12.3	4.06

Dose Rate / Concentration

	K(+Rb) (mGy/a/%K)	U (mGy/a/ppmU)	Th (mGy/a/ppmTh)
Alpha		2.78	0.739
Alpha Eff (a=0.15)		0.417	0.111
Beta	0.830	0.146	0.0286
Gamma	0.241	0.115	0.0514

Shap Granite Working Values

Concentration

K (%)	U (ppm)	Th (ppm)
4.43 ± 0.03	12.0 ± 0.06	28.5 ± 0.26

Specific Activity

K (Bq/kg)	238-U (Bq/kg)	232-Th (Bq/kg)
1370 ± 10	148.2 ± 7.4	115.6 ± 1.05

Table 2.2. Activity and dose rate conversion factors for K, U and Th, and working values for the Shap Granite reference material used in laboratory gamma spectrometry measurements. Conversion factors are from Aitken (1983). Effective alpha conversion was calculated assuming alpha efficiency to be 0.15. Working values for Shap Granite are based on Sanderson (1986).

Infinite matrix dose rates were calculated from the parent concentrations illustrated in Figure 2.5, using the conversion factors in Table 2.2. From these were calculated the effective dose rate from each sample's matrix, to two of the grain size separates used to measure the luminescence signal and hence D_e (Eqn. 1), when dating sediments: polymineral fine grains (4-11 μm diameter), and hydrofluoric-etched sand-sized grains (etched core assumed to be 200 μm in diameter).

The polymineral fine grains are small enough to receive the full dose rate from alpha, beta, and gamma radiation, but the lower relative efficiency of alpha radiation in producing a luminescence signal needs to be taken into account. The effective infinite matrix dose rate to polymineral fine grains is thus the sum of the beta, gamma, and effective alpha dose rates.

The sand sized grains are small enough to receive the full dose rate from gamma and beta, but alpha radiation only penetrates the outer few μm of the grains. Etching in hydrofluoric acid is designed to remove this layer, so that the core has not received an external alpha dose. However the etched layer (assumed to be ~10 μm) is thick enough to have absorbed some of the beta dose rate. The fraction penetrating to the core of the grain depends on the energy of the beta radiation: the average values for K, U, and Th used in the present study were 0.93, 0.85, and 0.79 respectively. The

infinite matrix dose rate to etched 200 μm grains is thus the sum of gamma and the fraction of beta absorbed in the core. The internal dose rate of the grains has not been considered at this stage, but is likely to become a significant factor if the matrix dose rate is much below 1 mGy/a.

2.2 Gamma Spectrometer Performance

In order to understand any measurement related effects in the results from the EFCHED samples, detector performance through the period in which the samples were measured was first assessed by examining the results obtained from measurements of background and the Shap reference material. Figure 2.2 shows total count rates, summed across all the regions of interest in Table 2.1, for each measurement of background, Shap, and sample, in order of measurement, on each detector.

The data in Figure 2.2 indicate that:

1. Shap and background response vary by up to ~5%, but there do not appear to be significant trends with time during this measurement period.
2. The radioactivity of the EFCHED samples is much closer to background than to that of the Shap reference material, but is highly variable.
3. Count rates from Detector 2 were ~1/3 higher than from Detector 3, but appear slightly more scattered.

Since there did not appear to be significant trends in total detector response with time during the measurement period, it was considered appropriate to average the Shap and background measurements in order to improve counting statistics for each of the individual emission peaks measured. Measurement times varied, so the weighted mean of the count rates was taken (Figure 2.3 a. and b.). Uncertainties were calculated as the "internal" and "external" error on the weighted mean (α_i Eqn. 3, α_e Eqn. 4).

Eqn. 3.
$$\alpha_i^2 = \frac{1}{\sum_{i=1}^{n} 1/se_i^2}$$

Eqn. 4.
$$\alpha_e^2 = \frac{\sum_{i=1}^{n} (x_i - \bar{x})^2 / se_i^2}{(n-1)\sum_{i=1}^{n} 1/se_i^2}$$

The "internal" error is propagated through the calculation of weighted mean from counting statistics, but the "external" error also includes a contribution from scatter between the data. The ratio of these values for each emission peak is shown in Figure 2.3 c. and d., to indicate the level of scatter in the data that cannot be explained by counting statistics. The ratio of signal levels obtained from Shap and background are plotted in Figure 2.3 e. and f., with expected error.

The data in Figure 2.3 indicate that:

1. The largest signals from Shap correspond to the highest intensity emissions in Table 2.1, while the largest background signals are found in the lower energy peaks, associated with the Compton continuum.

2. Scatter beyond that explained by counting statistics was much greater in the results from Detector 2 than those from Detector 3, while on an emission-emission basis it appeared greatest for the post-radon peaks in the Uranium series.
3. Signal levels from Shap were generally around an order of magnitude above background, the exceptions being the low energy peaks in the Uranium series, and the 2.6 MeV ^{208}Tl peak in the Thorium series.

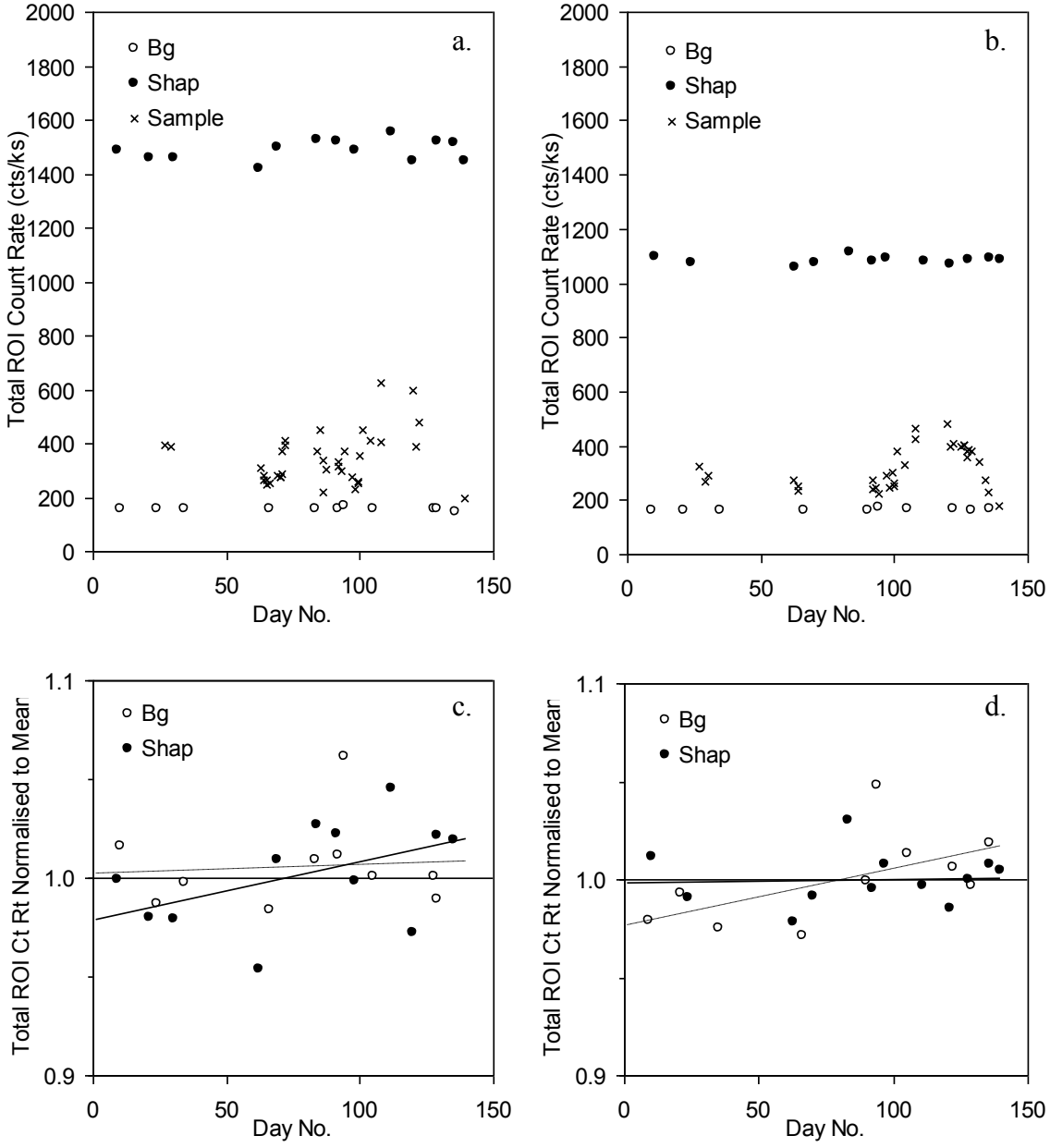

Figure 2.2. Reference (Shap and background) and sample count rates through the period of measurements for Detector 2 (a. and c.), and Detector 3 (b. and d.). Total count rates, summed across the regions of interest, are shown in a. and b. Total count rates normalised to their mean values are shown in c. and d., to illustrate trends in Shap and background response through the period of the measurements.

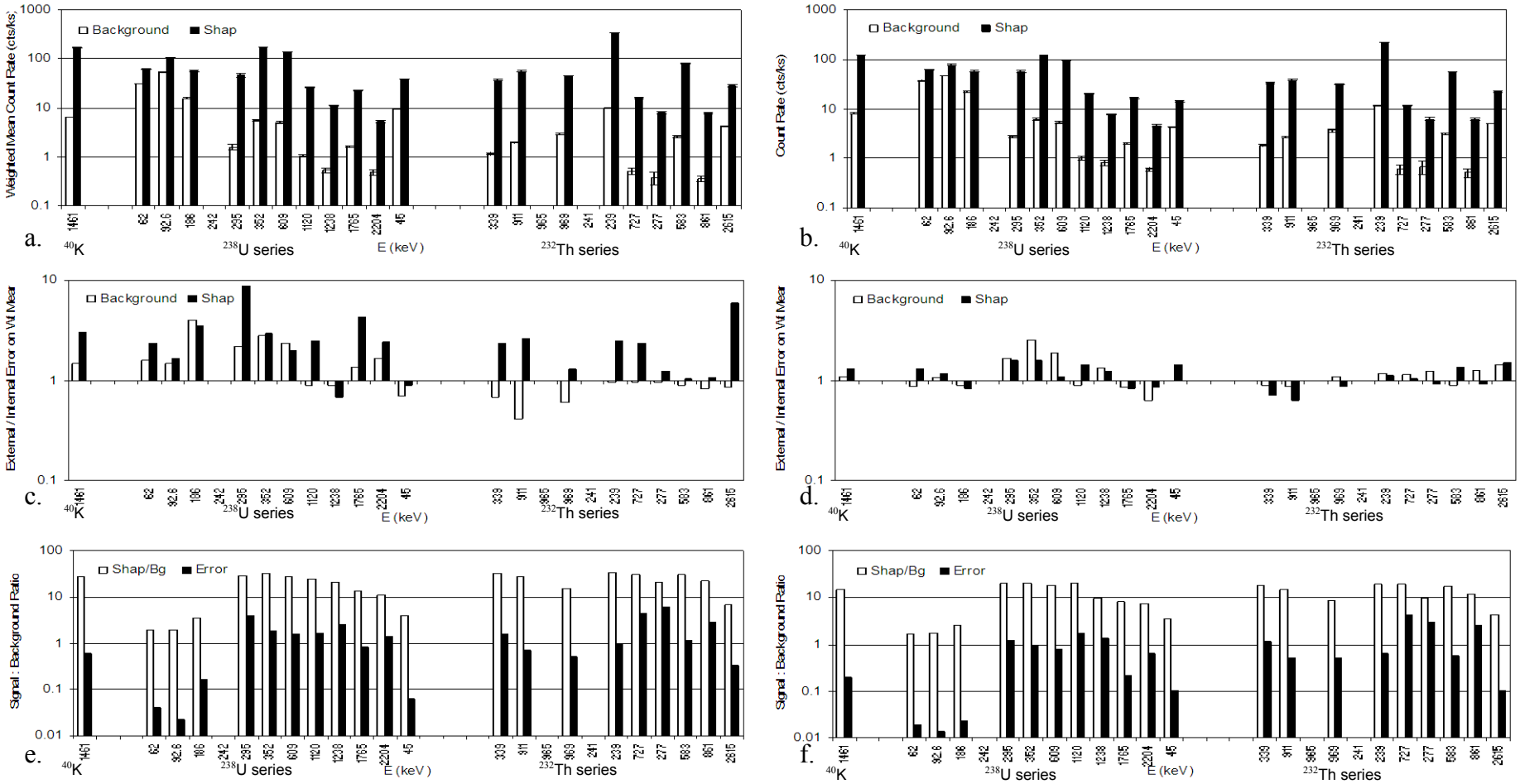

Figure 2.3. Reference (Shap and background) weighted mean count rates in individual regions of interest (ROI), across the period of measurement (a. and b.). "External" and "internal" errors on the weighted means (Eqn. 3, Eqn. 4) are compared in c. and d. to indicate the proportion of scatter in the data that cannot be explained by counting statistics. Variations in signal:background ratio between different ROIs are illustrated in e. and f. a., c., and e. are data from Detector 2, b., d., and e. are data from Detector 3. Labels on the x-axes are energies associated with each emission peak (ROI). Note logged y-axes.

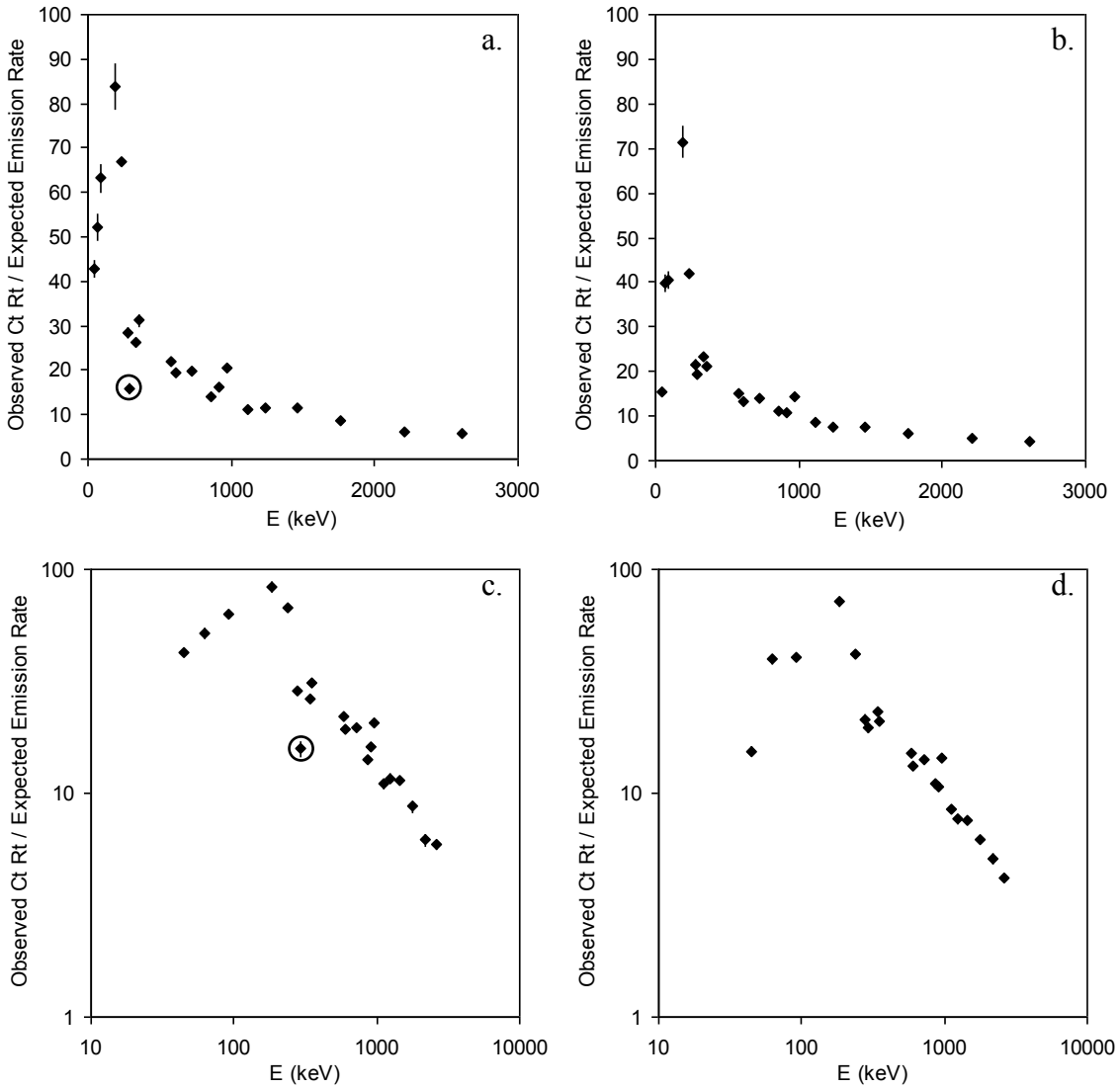

Figure 2.4. Apparent detector efficiency vs. emission peak energy. a. and c. are data from Detector 2, b. and d. are data from Detector 3. The circled datapoint in a. and c. is the 295.2 keV emission from ^{214}Pb.

Higher signal levels but greater scatter, and a greater proportion not explained by counting statistics, indicated that Detector 2 was more efficient but less stable than Detector 3. To assess this directly the observed count rate from each peak was compared with its expected emission rate for the Shap Granite reference material (Figure 2.4), taking into account the approximately 2π geometry of the detection system. Expected emission rates were calculated by multiplying the specific activities of the parents (Table 2.2) by the mass of the Shap (0.1 kg), by the intensity of each emission (Table 2.1), and in the case of the ^{208}Tl peaks, by its branching ratio with ^{212}Po (0.36).

The data in Figure 2.4 indicate that:

1. Detector efficiency increases as the energy of emission decreases to ~200 keV, according with the expectation that at high energies less of the gamma ray photons will interact inside the finite volume of the detector. Also, below 200 keV detector efficiency decreases due to absorption within the sample volume.

2. Trends in apparent efficiency with emission energy are generally consistent from peak to peak, but the Detector 2 data exhibit more scatter than Detector 3, and the 295.2 keV emission from ^{214}Pb is not consistent with the general trend from Detector 2.
3. The apparent efficiency of Detector 2 (Figure 2.4 a. and c.) is generally around 30 % higher than that of Detector 3 (Figure 2.4 b. and d.), reflecting the difference in count rate observed in Figure 2.2.

The patterns in detector response described above are considered to indicate that the regions of interest used for Detector 2 were not as appropriate as those used for Detector 3. With reference to Table 2.1., it is apparent that the ROIs used for Detector 2 were sometimes slightly narrower than those used for Detector 3. This may have led to imprecise determination of the continuum level under each peak, and hence imprecise determination of peak counts. In extreme cases it could also lead to incomplete peak counting: in particular, the 295.2 keV emission from ^{214}Pb, although the 295.2 keV emission is the weaker of those measured from ^{214}Pb and should not dominate pooled results incorporating it. However, it is unclear why apparent detection efficiency would be improved by using narrower ROIs.

2.3 Parent Concentrations

The weighted means of count rates from background and the Shap reference sample were calculated for each ROI across the period during which the EFCHED samples were measured. Background count rates were then subtracted from Shap and sample count rates, and the sample count rates scaled to count rate per unit concentration in the Shap (Eqn. 2, Table 2.2). This yielded apparent parent concentrations for each ROI, from which were calculated the weighted mean parent concentration for each parent element (assuming equilibrium, Figure 2.5) and for each isotope in the U and Th decay series (Figure 2.6). For comparison, specimen contexts are often assumed to have parent concentrations of 1 % K, 1 ppm U, and 3 ppm Th (e.g. Adamiec and Aitken, 1998). Although these assumptions ultimately relate to the TL dating of pottery, any approximations necessary in the determination of conversion factors etc. are expected to have been made on the basis that such a "typical" context is being examined. The 3:1 ratio between Th and U results in approximately equal radioactivities in the two decay series, so deviations from this indicate when one is a more important contributor to dose rate than the other.

To illustrate the relative amounts of Potassium, Uranium and Thorium in the EFCHED samples, and variations in one relative to another, Parent Concentration is plotted on a log-axis in Figure 2.5a., and the Th:U ratio is plotted separately in Figure 2.5b.. The data in Figure 2.5 indicate that:

1. Concentration of Potassium in the EFCHED samples is commonly around 1 %, but ranges from 0.03 to 3.5 %. Concentration of Uranium is commonly around 2 ppm, but ranges from 0.4 to 3.3 ppm. Concentration of Thorium is commonly around 5 ppm, but ranges from 0.3 to 11 ppm. The concentrations in some of the EFCHED samples therefore deviate from the specimen context noted above, by up to an order of magnitude.
2. Concentrations are highest at Malaya Voronsovskaya, Akhshtyr, Kepshinskaya (clayey limestone cave sites), and Biriuchya Balka

(loessic, open site). Concentrations are lowest at Kalitvenka (quartzite open site) and Kabazi V (limestone cave site).

3. The greatest proportional scatter in concentration within a site occurs in some of the rocky limestone cave sites of the Northern Caucassus, but the largest proportional change in dose rate down section occurs at the open site of Kalitvenka, as "clean" quartzite sand progresses to sediments of mixed content.
4. Within each site, trends in concentration down section are usually similar for each parent element. K is generally a constituent of mineral grains, so similar trends in U and Th indicate that these may also be mainly within grains, and therefore not especially mobile. However, U often appears to vary by a lesser proportion than K and Th. This indicates that some of the U is not fixed with the K and Th, and may have moved. Sites where this is particularly obvious are Gubs Rockshelter 1, Akhshtyr, Kostienki 14, and Kabazi II.
5. The ratio of Th to U in the EFCHED samples is commonly around 3, but ranges from 0.9 to 5.0. The only values much above 3 are found in the clayey contexts of Akhshtyr and Kepshinskaya (limestone caves). Values well below 3 are found throughout Kabazi II and V, and less consistently at Monasheskaya and Gubs Rockshelter 1, and Kalitvenka. In the case of Kalitvenka there are large uncertainties on the low Th/U values because they are derived from very low values of concentration (<0.5 ppm Th and U).

Apparent parent concentrations of natural Uranium and Thorium, based on gamma spectrometry results from individual isotopes in the ^{238}U and ^{232}Th decay series, are plotted in Figure 2.6 a. and b. respectively. Differences between values calculated from different isotopes can indicate disequilibrium and/or differences in detector performance.

The data in Figure 2.6 a. (^{238}U series) indicate that:

1. ^{214}Pb and ^{214}Bi values exhibit much less scatter than the other isotopes: they are determined from multiple emissions in the mid-high energy range, whereas values for the other isotopes are determined from fewer emissions, all below 200 keV (Table 2.1). At lower energies the signal to background ratio is low, even if signal levels are high (Figure 2.3).
2. Although more scattered, ^{234}Th and ^{226}Ra values are generally similar to those of ^{214}Pb and ^{214}Bi, indicating that the pots used for gamma spectrometry measurements were generally well sealed. Gaseous ^{222}Rn lies between ^{226}Ra and ^{214}Pb in the decay series, and ^{214}Pb has a 26 minute half life, so any radon escape would have to occur during measurement to cause large differences. Samples where ^{234}Th and ^{226}Ra were both clearly higher than ^{214}Pb and ^{214}Bi were; 1589 (Monasheskaya), 1631 (Biriuchya Balka 2), 1666, 1667 (Kabazi V), 1685, 1686, 1687 (Karabai). However, U concentrations for these samples, calculated assuming the presence of the full series, do not appear low compared to similar/nearby samples, nor do the Th/U ratios appear high (Figure 2.5).
3. Although scattered, the ^{210}Pb values commonly appear lower than from the other isotopes, which is indicative of ^{222}Rn movement in

the last few decades. It is most obvious at Gubs Rockshelter 1, Navalishenskaya, and Malaya Vorontsovskaya, but also in the lower levels of Kalitvenka 1, the South section of Kostienki 14, Kabazi V, and the lowest levels of Kabazi II. However, the ^{210}Pb values were determined from a single, very low energy emission, so measurement related effects may have a substantial effect on the apparent parent concentration from this isotope.

4. ^{226}Ra sometimes differs noticably from ^{234}Th, and the isotopes further down the decay series. This is indicative of the movement of Uranium and/or Radium (in solution). At Gubs Rockshelter 1, Navalishenskaya, Malaya Vorontsovskaya, and in the upper layers of section У-Г at Monasheskaya, ^{226}Ra is generally higher than ^{234}Th. In the lower levels at Kalitvenka and the lower levels at Kabazi V, ^{226}Ra is lower than ^{234}Th.

The data in Figure 2.6 b. (^{232}Th series) indicate that:

1. The level of ^{228}Ac in the Russian Steppe sites (Biriuchya Balka, Kalitvenka, Kostienki) is often greater than the level of ^{208}Tl. ^{228}Ac and ^{208}Tl are expected to have the best known values of the isotopes in the ^{232}Th series, having been determined from four emissions each, over a range of energies. It is possible for disequilibrium to occur between these isotopes, by movement of ^{224}Ra and/or ^{220}Rn, but the short half lives of these isotopes mitigate against this. In the other sites ^{228}Ac and ^{208}Tl levels are generally similar: only sample SUTL1621 from Akhshtyr appears to have particularly high levels of ^{228}Ac, and it also has a high Th/U ratio.
2. ^{212}Bi commonly, but not at all sites, exhibits more scatter than the other isotopes. It is determined from a single relatively low intensity emission, albeit at relatively high energy.
3. Other than this there do not appear to be consistent differences between the results from the different isotopes.

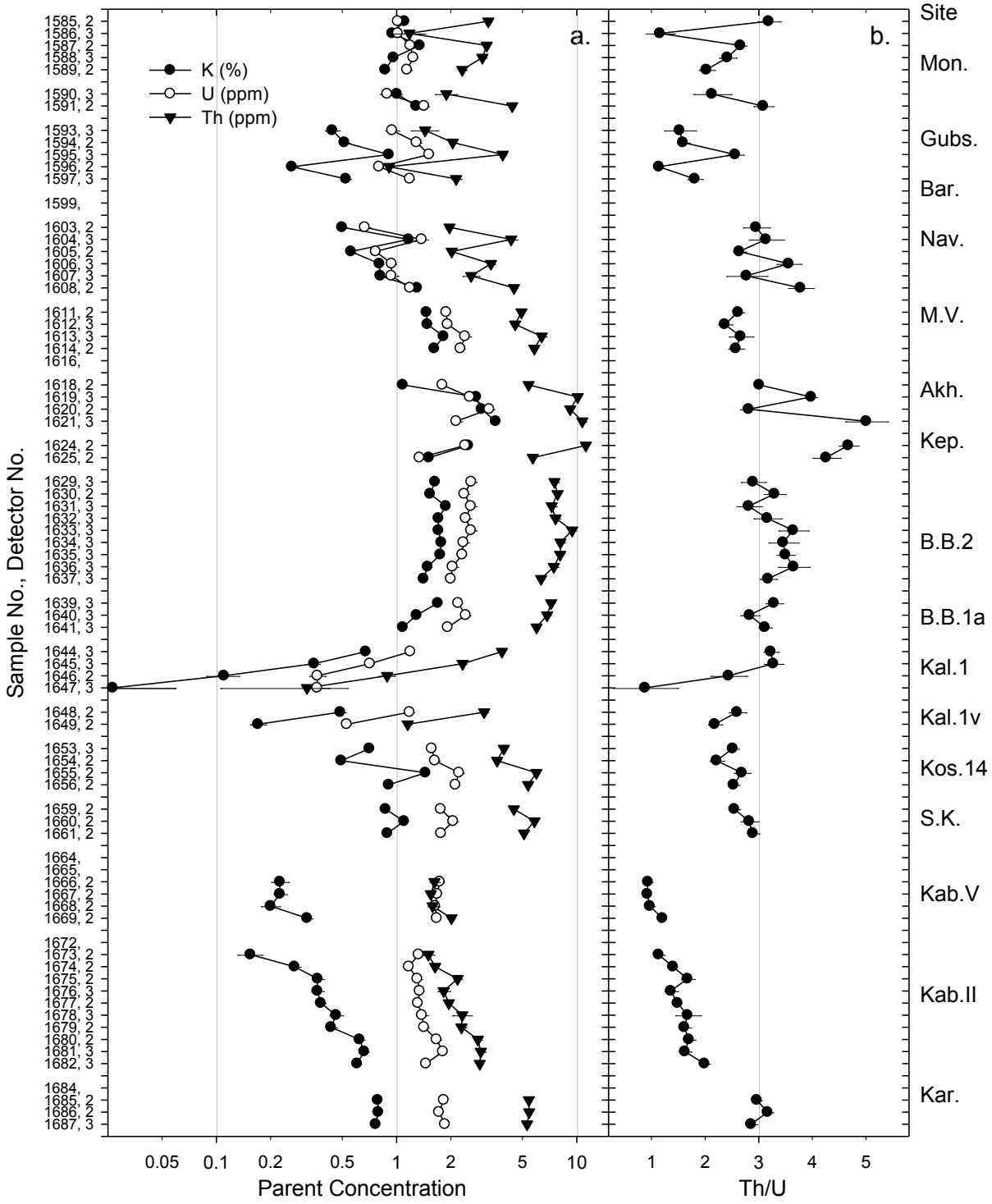

Figure 2.5. Elemental concentrations of K, natural U and natural Th in each sample (a.). Values were calculated as the weighted mean of results from the emissions measured using gamma spectrometry, and calculated assuming secular equilibrium. Note logged axis. b. Ratio of Thorium to Uranium. Sample (SUTL) number, and the detector with which the sample was measured, are indicated on the left axis. The site to which each group of samples belong, in stratigraphic order, is indicated on the right.

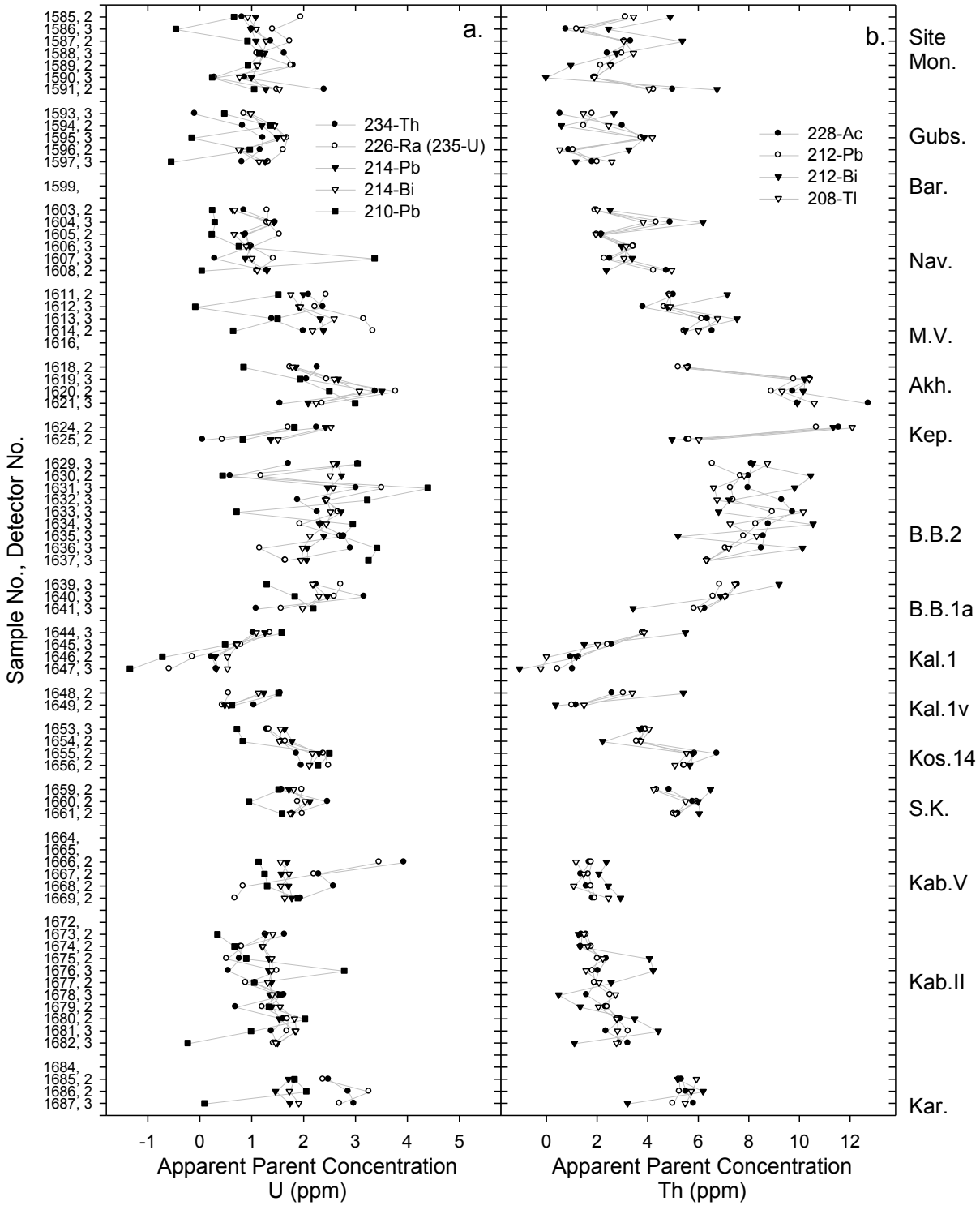

Figure 2.6. Elemental concentrations of U (a.) and Th (b.) indicated by each isotope measured in the respective decay series. Where more than one emission was measured per isotope the values are weighted means. Sample (SUTL) number, and the detector with which the sample was measured, are indicated on the left axis. The site from which each group of samples was taken is indicated on the right.

2.4 Dose rates

Weighted mean parent concentrations (calculated assuming equilibrium, Figure 2.5), were used to calculate the infinite matrix dose rate to the fine (4-11 μm) and coarse (acid etched 200 μm) grains used for D_e determination (section 2.1). These values are presented, for each of the EFCHED samples, in Figure 2.7 and Figure 2.8, with the relative contributions of each parent element, and each type of radiation.

The data in Figure 2.7 (fine grains) indicate:

1. Total infinite matrix dose rate to fine grains ranges from 0.33 to 7.29 mGy/a, but commonly lies between 1.5 and 4.5 mGy/a. The highest dose rates were observed for Malaya Vorontsovskaya, Akhshtyr, Kepshinskaya, and Biriuchya Balka, the lowest at Kalitvenka.
2. Scatter between samples is greatest at Monasheskaya, Gubs Rockshelter 1, Navalishenskaya, and Kostienki 14, but gradual trends in dose rate down section at other sites are often of greater magnitude than this scatter.
3. The Thorium contribution to total dose rate was generally the lowest, but the most consistent of the three parent elements (Figure 2.7 b). Potassium and Uranium contributions were more variable: one generally varied as the inverse of the other. Uranium was dominant at Kabazi (V and II) and in the lower levels at Kalitvenka, but was slightly higher than K or Th at Gubs Rockshelter 1, Kostienki 14, and Sari Kaya. Potassium was the greater contributer at Monasheskaya, Navalishenskaya, Malaya Voronsovskaya, Akhshtyr and Kepshinskaya.
4. The gamma contribution was very consistent around 21.4% in all cases (Figure 2.7 c). The alpha contribution was almost twice as large (40%), as well as more variable, being higher for the sites/samples with a greater Uranium contribution. Beta contributed a similar percentage of dose rate as alpha, but less for the sites with a greater Uranium contribution.

The data in Figure 2.8 (coarse grains) indicate:

1. Total infinite matrix dose rate to coarse grains ranges from 0.14 to 4.9 mGy/a, but commonly lies between 1 and 3 mGy/a. Patterns in magnitude and scatter were similar to those for the fine grains.
2. The Potassium contribution is enhanced relative to the fine grain values, since the coarse grain dose rate does not include a contribution from alpha radiation. Thus, the Uranium and Thorium contributions are generally similar, around 20% at many of the sites, where Potassium is around 50-60%. The Uranium contribution was much higher than Thorium at Gubs Rockshelter, Kalitvenka, and Kabazi II and V, but dominated over Thorium and Potassium only at Kabazi V, in the upper layers of Kabazi II, and the lowest layers at Kalitvenka.
3. Since the etched coarse grains receive no external alpha dose rate, beta and gamma contributions mirror each other, but are relatively consistent around 61 % and 39 % respectively (Figure 2.8 c). The highest gamma contributions are at Kalitvenka and Kabazi, the lowest at Monasheskaya.

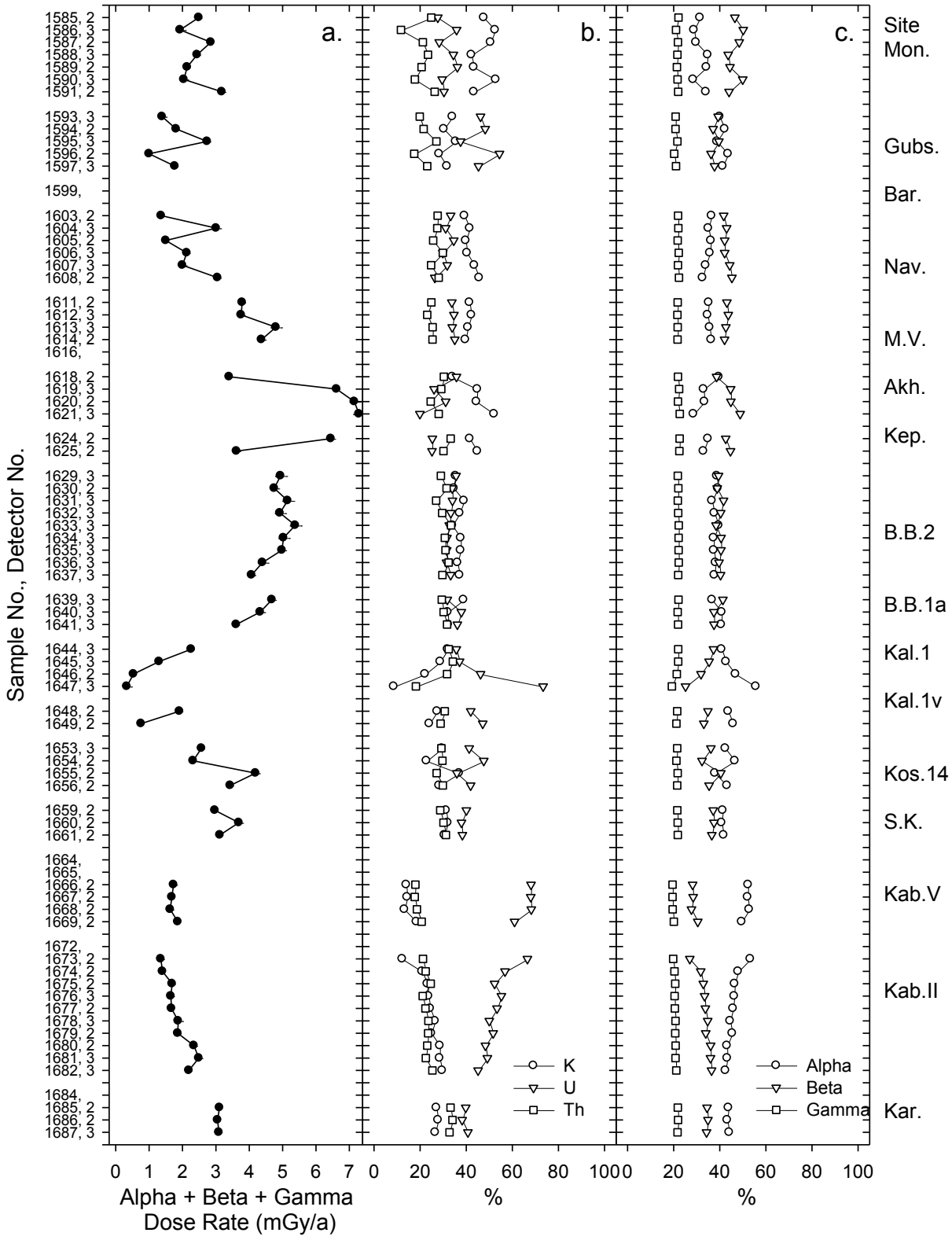

Figure 2.7. Infinite matrix (dry) dose rate to polymineral fine grains (4-11 μm) from radioisotopes in each sample (a.). b. % from K, U, and Th. c. % from alpha, beta and gamma radiation. Sample (SUTL) number, and the detector with which the sample was measured, are indicated on the left axis. The site from which each group of samples was taken is indicated on the right.

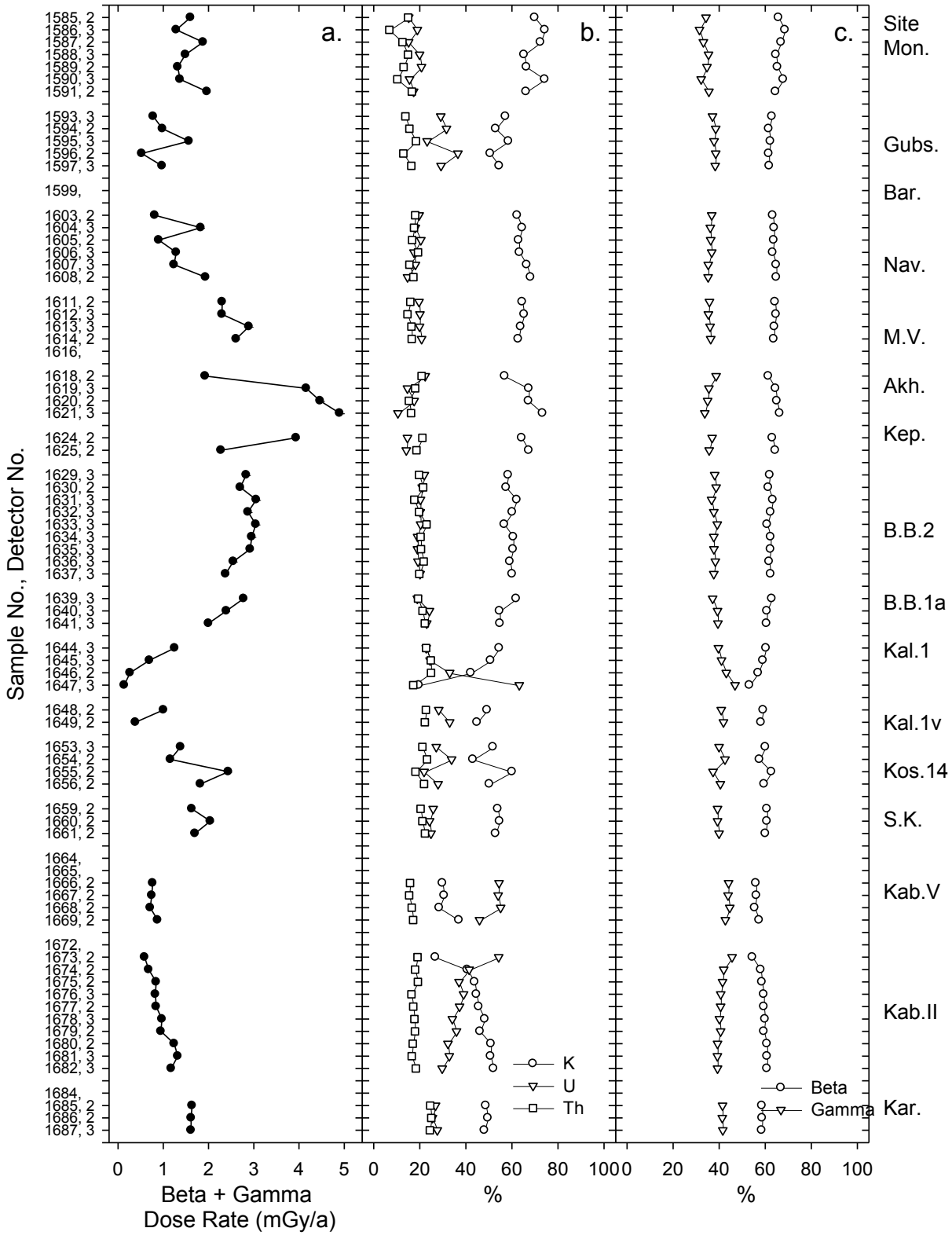

Figure 2.8. Infinite matrix (dry) dose rate to etched sand sized grains of quartz (~200 μm) from radioisotopes in each sample (a.). b. % from K, U, and Th. c. % from beta and gamma radiation. Sample (SUTL) number, and the detector with which the sample was measured, are indicated on the left axis. The site from which each group of samples was taken is indicated on the right.

% total dose rate	4-11 μm Mean	SD	etched 200 μm Mean	SD
K	33	10	55	12
U	40	12	27	11
Th	26	5	18	4
Alpha	40	6	-	-
Beta	38	6	61	3
Gamma	21.4	0.8	39	3

Table 2.3. Average percentage contribution to total infinite matrix doserate, to fine grains and etched coarse grains in the EFCHED samples.

2.5 Comparison of laboratory and field gamma spectrometry results

Many of the sampled sediments appeared inhomogeneous on the cm to dm scale. In the field it was attempted to take samples for laboratory gamma spectrometry that would be representative of the luminescence samples' immediate environments. However, in many cases it was expected that the variable presence of limestone clasts and/or context boundaries close to the sample might produce differences between field and laboratory gamma dose rate determinations. In other sites, e.g. Biriuchya Balka, the deposits appeared relatively homogeneous, and the field and laboratory results were expected to be similar.

In order to compare field and laboratory gamma dose rate determinations, the laboratory measurements were first corrected for the *in-situ* water contents measured from those samples prior to milling (Eqn. 5; Aitken, 1985). Both gamma dose rates are plotted together in Figure 2.9, with the ratio of field to lab' gamma dose rate, and the *in-situ* water content for each of the EFCHED samples.

Eqn. 5. $$D_{\gamma insitu} = D_{\gamma dry} / (1 + 1.14 M_{water} / M_{sediment})$$

The data in Figure 2.9 indicate that:

1. Similar patterns are observed in both laboratory and field gamma dose rate, between sites, and down section within sites. However, laboratory gamma dose rate is higher than the field measurements for all but two samples, and generally exhibits greater scatter between the contexts of a given site.
2. Lab' gamma dose rate is most scattered within the limestone sites of Monasheskaya, Gubs Rockshelter 1, and Navalishenskaya, although other sites exhibit trends in dose rate down section that are of greater magnitude. However at other apparently inhomogeneous sites, e.g. Kabazi, levels of variability are similar to the more homogeneous sites such as Biriuchya Balka.
3. Scatter in field gamma dose rate, as distinct from trends down section, appears similar for all sites, whether apparently homogeneous or not.

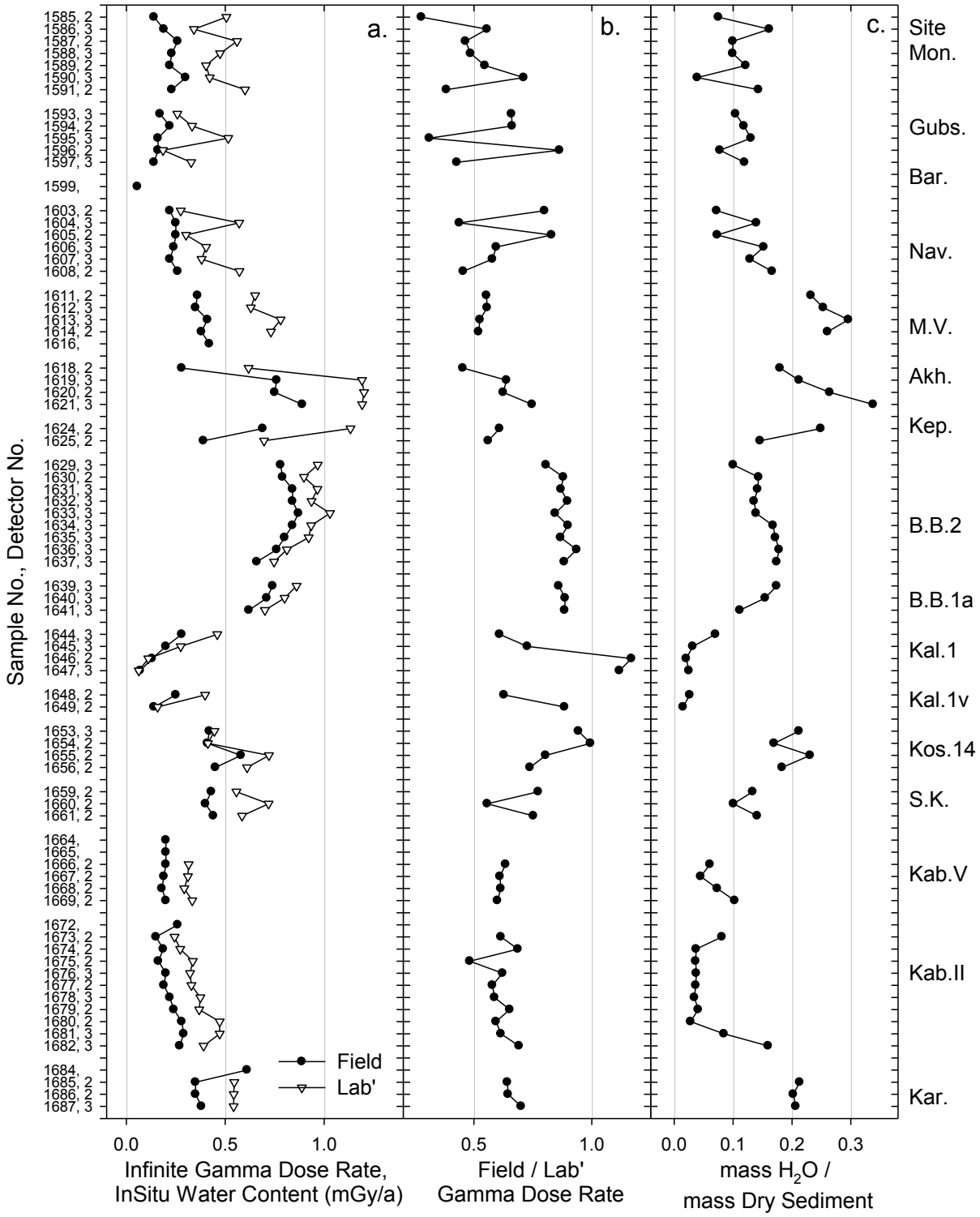

Figure 2.9. Gamma dose rates measured *in-situ* using a portable NaI gamma spectrometer and using 100 g samples and a high resolution Ge system in the laboratory (a.). b. Ratios of field to laboratory value. Field measurements have been corrected for *in-situ* water content, which is plotted in c.. Sample (SUTL) number, and the detector with which the sample was measured, are indicated on the left axis. The site from which each group of samples was taken is indicated on the right.

4. Field gamma dose rate is commonly between 0.5 and 0.7 times the laboratory value, but the ratio ranges from 0.28 to 1.17. The ratio is commonly closer to 1 for the open sites of the Russian Plain. Ratios below 0.5 only occur in contexts where the presence of limestone clasts or bedrock are likely to have made the laboratory measurement unrepresentative.
5. Water content ranged from 0.02 to 0.34 of the samples' dry sediment masses. Although some of the sections had been exposed for some time before sampling, while others were freshly re-exposed, water content still broadly reflects the texture of the *matrix* of the sediments: higher = finer, lower = coarser.
6. There appears to be a positive relationship between gamma dose rate and water content, which may relate to matrix texture (i.e. silt and clay content). However, there does not appear to be a relationship between water content and the ratio of field to lab' gamma dose rate.

2.6 Summary and discussion of gamma spectrometry survey results

Assessment of the performance of the two detectors used for lab' gamma spectrometry indicated that total count rates from the background and Shap reference material varied by no more than 5% during the period the samples were measured, with no observed trends in efficiency through time. Detector 2 was found to be more sensitive but less stable than Detector 3, based on count rates from individual peaks: there was rather more scatter in the results than could not be explained by counting statistics alone. It was also noted that signal to background ratios were much poorer for emissions below ~200 keV than those at higher energies, and that count rates from the EFCHED samples were closer to background than to the Shap reference material.

Parent concentrations of K, U, and Th varied by an order of magnitude between the EFCHED samples, but relative levels of K:U:Th were commonly similar to expected values from specimen contexts. Both the highest and some of the lowest radionuclide concentrations were found in limestone rich sites. The high concentrations were from clayey deposits at Akhshtyr, Kepshinskaya, and Malaya Voronsovskaya in the Sochi region (Figure 2.5; Burbidge *et al*., 2005, Chapter 3). These deposits often contained limestone clasts, but the fine matrix did not appear to have weathered from the clasts, which appeared to be roof fall probably resulting from frost action. The lab' gamma spectrometry sample therefore consisted mostly of fine matrix material. Of these sites, Akhshtyr and Kepshinskaya yielded the highest Th/U ratios of all the EFCHED samples. By contrast, very low parent concentrations and very low Th/U ratios were observed at Kabazi II, Kabazi V, and Gubs Rockshelter 1. The sediments at these sites generally appeared colluvial in nature and contained large amounts of worn / weathered limestone. They were also relatively low in K, such that any Uranium series disequilibrium would have a relatively large impact on the determination of the average dose rate to the archaeological samples. The lowest parent concentrations in the EFCHED samples were observed at Kalitvenka, in deposits of clean quartzite sand. Th/U ratios were also low in these layers, but with large uncertainties.

Examination of results from different isotopes in the ^{238}U series showed how the pooled determination of parent concentration depended strongly on the post-radon isotopes ^{214}Pb and ^{214}Bi. It also indicated possible radon escape during measurement

from samples 1589 (Monasheskaya), 1631 (Biriuchya Balka 2), 1666, 1667 (Kabazi V), 1685, 1686, 1687 (Karabai). These samples will need to be recounted and possibly resealed for dose rate determinations to produce dates. There were also limited indications of Uranium and/or Radium mobility at Gubs Rockshelter 1, Navalishenskaya, Malaya Vorontsovskaya, in the upper layers of section У-Г at Monasheskaya, and in the lower levels at Kalitvenka and Kabazi V. However, when the ^{232}Th series was examined, limited indications of disequilibrium were also observed, in this case at the Russian Plains sites. The mobility of some of the isotopes in the ^{232}Th decay series is not expected to manifest itself, as a result of their short half lives and consequently short window for movement. It may therefore be that the limited indications of disequilibrium in both the Thorium and Uranium decay series are artefacts of measurement.

Infinite matrix dose rates calculated from weighted mean parent concentrations, assuming equilibrium, ranged from 0.25 to 6.34 mGy/a for fine (silt-sized), and from 0.14 to 4.9 mGy/a for etched coarse (200 μm) mineral grains in the sediment. On average the fine grain dose rate was around 1.5 times the coarse grain dose rate, so more luminescence signal might be expected from fine grains, but saturation effects would also be observed in younger samples. Comparison of the contributions to dose rate showed how α radiation, and hence the U series, contributes more strongly to the fine grain dose rate, while γ radiation, and hence K, contributes more strongly to the coarse grain dose rate. This makes fine grain dose rates more susceptible to U series disequilibrium as well as variations in α efficiency. Patterns in infinite matrix dose rate through the sites followed those of the parent concentrations discussed above, such that the U series contributed most strongly at Gubs Rockshelter, Kalitvenka, and Kabazi II and V, making these sites most susceptible to the effects of disequilibrium.

The greater scatter observed in lab' gamma spectrometry results compared to field measurements at less homogeneous sites indicates that the samples taken for laboratory measurements were not always representative of their wider gamma environment. This would make the field values of gamma dose rate preferable for use in age determinations. However, at more homogeneous sites the field measurements consistently underestimated the lab' values. The laboratory determinations are expected to be more accurate for a given sample, and the calibration of the field gamma spectrometer is presently under review.

References

Adamiec, G., and Aitken, M. J. (1998). Dose-rate conversion factors: update. *Ancient TL* 16, 37-49.

Aitken, M. J. (1983). Dose rate data in SI units. *PACT* 9, 69-76.

Aitken, M. J. (1985). "Thermoluminescence dating." Academic Press, London.

Beliaeva, E. V. (1999). "Mustierskii mir Gubskogo ushchelia (Severnyi Kavkaz) (The Mousterian world of the Gubs Gorge)." St. Petersburg.

Burbidge, C. I., Allsworth Jones, P., Housley, R. A., Sanderson, D. C. W., Pyle, D., Bazely, O., McCave, N., and van Andel, T. (2005). "Middle Palaeolithic sites in Russia and Ukraine: site summaries and fieldwork 2004." SUERC, University of Glasgow, Glasgow.

Chabai, V. P. (2004). "The Middle Palaeolithic of Crimea: stratigraphy, chronology, typological variability & Eastern European context." National Academy of Sciences of Ukraine, Archaeology Institute, Crimean Branch, Simferopol, Kiev.

Jacobs, Z., Duller, G. A. T., and Wintle, A. G. (2003). Optical dating of dune sand from Blombos Cave, South Africa: II- single grain data. *Journal of Human Evolution* 44, 613-625.

Krbetschek, M. R., Gotze, J., Dietrich, A., and Trautmann, T. (1997). Spectral information from minerals relevant for luminescence dating. *Radiation Measurements* 27, 695-748.

Lang, A. (1994). Infrared Stimulated Luminescence Dating of Holocene Reworked Silty Sediments. *Quaternary Science Reviews* 13, 525-528.

Liubin, V. P. (1989). Paleolit Kavkaza (Palaeolithic of [the] Caucasus). *In* "Paleolit Kavkaza i Severnoi Azii." pp. 8-142. Seria Paleolit mira, Leningrad.

Liubin, V. P., and Shchelinski, V. E. (1967). Investigation of Navalishenskaya cave in 1965 (in Russian). *Kratkie soobshcheniya Instituta arkheologii* 111.

Matiukhin, A. E. (1998). Les ateliers du paleolithique superieur de la vallee du Donets- Severski, region de Rostov, Russie. *L'Anthropologie* 102, 467-494.

Murray, A. S., and Wintle, A. G. (2000). Luminescence dating of quartz using an improved single-aliquot regenerative-dose protocol. *Radiation Measurements* 32, 57-73.

O'Brien, C., Plant, J. A., Simpson, P. R., and Tarney, J. (1985). The geochemistry, metasomatism and petrogenesis of the granites of the English Lake District. *Journal of the Geological Society of London* 142, 1139-1157.

Pyle, D. M., Ricketts, G. D., Margari, V., van Andel, T. H., Sinitsyn, A. A., Praslov, N. D., and Lisitsyn, S. (2006). Wide dispersal and deposition of distal tephra during the Pleistocene 'Campanian Ignimbrite/Y5' eruption, Italy. *Quaternary Science Reviews* 25, 2713-2728.

Roberts, H. M., and Wintle, A. G. (2001). Equivalent dose determinations for polymineralic fine-grains using the SAR protocol: application to a Holocene sequence of the Chinese Loess Plateau. *Quaternary Science Reviews* 20, 859-863.

Roberts, R. G., Galbraith, R. F., Olley, J. M., Yoshida, H., and Laslett, G. M. (1999). Optical dating of single and multiple grains of quartz from jinmium rock shelter, northern Australia, part 2, Results and implications. *Archaeometry* 41, 365-395.

Sanderson, D. C. W. (1986). Luminescence Laboratory Internal Report. SURRC.

Sanderson, D. C. W., Bishop, P., Houston, I., and Boonsener, M. (2001). Luminescence characterisation of quartz-rich cover sands from NE Thailand. *Quaternary Science Reviews* 20, 893-900.

Sinitsyn, A. A. (2003). The most ancient sites of Kostenki in the context of the Initial Upper Paleolithic of northern Eurasia. *In* "The Chronology of the Aurignacian and of the Transitional Technocomplexes. Dating, Stratigraphies, Cultural Implications." (J. Zilhão, and F. d'Errico, Eds.), pp. 89-107. Trabalhos de Arqueologia 33 - Proceedings of Symposium 6.1 of the XIVth Congress of the UISPP.

Stokes, S. (1994). The Timing of Osl Sensitivity Changes in a Natural Quartz. *Radiation Measurements* 23, 601-605.

Uthmeier, T. (2004). Transformation analysis and the reconstruction of on-site and off-site activities: methodological remarks. *In* "The Palaeolithic of Crimea, volume 3." (V. P. Chabai, K. Monigal, and A. E. Marks, Eds.), pp. 482. ERAUL 104, Liege.

Wintle, A. G. (1977). Detailed study of a thermoluminescent mineral exhibiting anomalous fading. *Journal of Luminescence* 15, 385-393.